Liquid Crystals
Publication details, including instructions for authors and subscription information:
http://www.informaworld.com/smpp/title~content=t713926090

Collective and antiferroelectric dielectric modes in a highly tilted three-ring ester

StanisŁaw A. Różański[a]; Jan Thoen[a]
[a] Laboratorium voor Akoestiek en Thermische Fysica, Departement Natuurkunde en Sterrenkunde, Katholieke Universiteit Leuven, B-3001 Leuven, Belgium

To cite this Article Różański, StanisŁaw A. and Thoen, Jan(2007) 'Collective and antiferroelectric dielectric modes in a highly tilted three-ring ester', Liquid Crystals, 34: 4, 519 — 526
To link to this Article: DOI: 10.1080/02678290701211561
URL: http://dx.doi.org/10.1080/02678290701211561

Liquid Crystals, Vol. 34, No. 4, April 2007, 519–526

Collective and antiferroelectric dielectric modes in a highly tilted three-ring ester

STANISŁAW A. RÓŻAŃSKI and JAN THOEN*

Laboratorium voor Akoestiek en Thermische Fysica, Departement Natuurkunde en Sterrenkunde, Katholieke Universiteit Leuven, Celestijnenlaan 200D, B-3001 Leuven, Belgium

(*Received 20 September 2006; accepted 7 December 2006*)

Broadband dielectric spectroscopy was applied to investigate a newly synthesized antiferroelectric liquid crystal, (*S*)-(+)-4′-(1-methylheptyloxycarbonyl)biphenyl-4-yl 4-(6-heptanoyloxyhex-1-oxy)benzoate. Near the SmA–SmC* phase transition the soft and the Goldstone modes are observed. The temperature dependence of the soft mode dielectric strength follows the Cure–Weiss law. In a narrow range of temperature the collective and antiferroelectric relaxation modes coexist as a result of the competition between ferroelectric and antiferroelectric order in the successive smectic layers. In the antiferroelectric SmC_a^* phase the low frequency, P_L, and high frequency, P_H, modes appear, which can be related to the in-phase and anti-phase azimuthal angle fluctuations of the director, respectively. The relaxation frequency of the P_H and P_L modes decreases linearly with decreasing temperature and satisfies the Arrhenius law. Some parameters involved in the extended Landau model of the SmA–SmC* phase transition could be obtained.

1. Introduction

Antiferroelectric liquid crystals (AFLCs) have attracted considerable attention during recent years as promising materials for applications in display technology [1]. AFLCs are a subclass of smectics in which the direction of the tilt and of the spontaneous polarization in successive layers point in opposite directions (anticlinic order), resulting in a lack of macroscopic spontaneous polarization in their antipolar and antiferroelectric SmC_a^* phase. Besides the SmC_a^* phase, other different chiral smectic C subphases can exist in these compounds, e.g. SmC_α^*, SmC_β^* or SmC_γ^*, as a result of the competition between synclinic and anticlinic order in neighbouring layers [2, 3]. However, the occurrence of many subphases is not always reproducible in AFLCs and depends on surface interactions, sample history or chemical and optical purity [4].

The electro-optic properties of surface-stabilized AFLCs differ considerably depending on the value of the tilt angle. The ordinary surface-stabilized AFLCs with a tilt angle value of about 25°–30° are optically positive biaxial crystals, with the effective optic axis lying along the smectic layer normal. In these materials the contrast ratio is unsatisfactory and light leakage is observed as a result of static and dynamic contributions to the dark state [5, 6]. However, it was shown that static and even dynamic light leakage are minimized using orthoconic AFLC materials (in which the directors in alternate layers are orthogonal) [6–8]. Intensive efforts were made to synthesize new unique AFLC compounds to improve electro-optic properties for future display applications [9–13]. It was shown that three-ring chiral esters having a $C_nF_{2n+1}COO(CH_2)_3O$ unit in one terminal chain exhibit smectic layers with anticlinic order and very large tilt [9–12]. In newly developed AFLC mixtures with a tilt angle of 45° [6–8, 14] in the antiferroelectric SmC_a^* phase, the crystal remains optically negative uniaxial with an effective optic axis perpendicular to the smectic layer normal. It behaves as an isotropic medium between crossed polarizers. For these materials the dark state extinction is limited only by the quality of the polarizers and is nearly completely independent of structural defects. Orthoconic AFLCs exhibit high spontaneous polarization and very short helical pitch [13, 14]. However, for technical applications the helical pitch should be at least 1 μm at room temperature (in the surface-stabilized state the helical superstructure should be unwound) which can be realized by adding achiral compounds or racemates [13].

The physical and electro-optical properties of AFLCs are intensively studied using various experimental

*Corresponding author. Email: Jan.Thoen@fys.kuleuven.ac.be

Liquid Crystals
ISSN 0267-8292 print/ISSN 1366-5855 online © 2007 Taylor & Francis
http://www.tandf.co.uk/journals
DOI: 10.1080/02678290701211561

techniques such as dielectric spectroscopy [15–22], electro-optics [23–25], X-ray diffraction [26, 27] and optical measurements [28, 29]. In particular, broadband dielectric spectroscopy (BDS) is a very powerful technique that enables one to determine the molecular and collective dynamics of the relaxation processes in very broad ranges of frequency and temperature. BDS allows characterization of the dynamics of the soft mode present in both the paraelectric SmA and the ferroelectric SmC* phases, as well as the Goldstone mode in the SmC* phase. Additionally, the P_L and P_H relaxation processes present in the antiferroelectric SmC_a^* phase can be investigated [16].

During the search for new AFLC compounds with very large tilt, several materials were synthesized possessing interesting electro-optic and dielectric properties [12]. These are chiral benzoates with a terminal group of the form R_1-$COOC_mH_{2m+1}O$, where $R_1=C_nH_{2n+1}$ ($n=6$ and 7) and $m=6$. In these materials the antiferroelectric SmC_a^* phase exists in a rather broad range of temperature. The dielectric properties of one of these AFLCs, with $n=6$, have already been investigated [30] and the main relaxation processes in different mesophases were assigned.

In the present work BDS is used to characterize the collective processes near the SmA–SmC* phase transition as well as the antiferroelectric modes in the SmC_a^* phase of the AFLC material with $n=7$. Moreover, the application of a bias electric field permitted better characterization of the dynamics of the soft mode, especially in the ferroelectric SmC* phase. The generalized Landau theory of the SmA–SmC* phase transition is applied to find the parameters involved in this model.

2. Experimental

The antiferroelectric liquid crystal (*S*)-(+)-4′-(1-methylheptyloxycarbonyl)biphenyl-4-yl 4-(6-heptanoyloxyhex-1-oxy)benzoate belongs to the new synthesized series of chiral benzoates with the formula shown in figure 1, where $R_1\equiv C_7H_{15}$ and $m=6$ [12]. This compound possesses besides the isotropic I, the paraelectric SmA and the ferroelectric SmC* phases, also an anticlinic SmC_a^* phase. The sequence of phase transition temperatures is:

$$\mathrm{Cr}(\leftarrow 311\ \mathrm{K})323.7\ \mathrm{K}\rightarrow \mathrm{SmC}_a^*\leftarrow 333.5\ \mathrm{K}\rightarrow$$
$$\mathrm{SmC}^*\leftarrow 344.9\ \mathrm{K}\rightarrow \mathrm{SmA}\leftarrow 355.2\ \mathrm{K}\rightarrow \mathrm{I}.$$

The antiferroelectric SmC_a^* phase can easily be supercooled to about 311 K. X-ray measurements of the temperature dependence of the smectic layer spacing show that the ratio d(SmC*)/d(SmA) attains in the SmC* phase a value of about 0.905 [12]. The estimated value of the tilt angle θ, from the simplified formula $\cos\theta = d(\mathrm{SmC}^*)/d(\mathrm{SmA})$, is about 25.2°.

The complex dielectric permittivity $\varepsilon^*(\omega, T)$ was measured in the frequency range 0.1 to 10^7 Hz using a Novocontrol broadband dielectric spectrometer, with a high resolution dielectric/impedance analyser Alpha and an active sample cell. The measurements were performed with bulk AFLC aligned homogeneously in 5 μm ITO cells, and in a measuring capacitor with gold-plated electrodes separated by 50 μm glass fibres. To achieve better orientation of the AFLC, the samples were slowly cooled from the isotropic to the SmA phase. It is well known that in ITO cells a spurious signal appears in the megahertz range with a frequency significantly dependent on the sample thickness and resistance of the ITO layer. Moreover, in the low frequency range the dielectric spectrum is disturbed by processes related to free charge carriers usually present in the LC. These unwanted signals overlap with the real relaxation processes present in the investigated material, but can be eliminated from the dielectric spectrum during a fitting procedure. Therefore, the experimental data can be evaluated using a superposition of Havriliak and Negami functions and spurious contributions discussed above in the form [16]:

$$\varepsilon^*(\omega, T) = \varepsilon_\infty + \sum_k \frac{\Delta\varepsilon_k}{\left[1+(\mathrm{i}\omega\tau_k)^{1-\alpha_k}\right]^{\gamma_k}} - \mathrm{i}\frac{\sigma_0}{2\pi\varepsilon_0 f^n} - \mathrm{i}Af^m, \quad (1)$$

where τ_k is the relaxation time and $\Delta\varepsilon_k$ the relaxation strength of the k-th absorption process. The exponents α_k and γ_k describe broadening and asymmetry of the relaxation time distribution, respectively. ε_∞ is the high

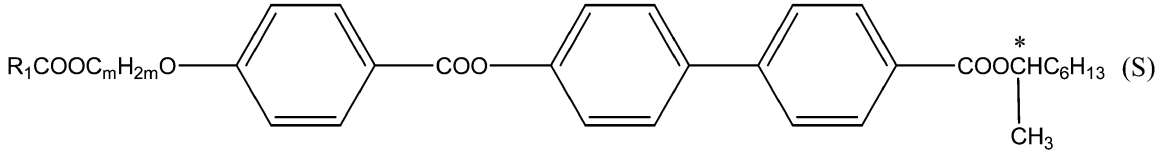

Figure 1. Chemical structure of the antiferroelectric liquid crystal (*S*)-(+)-4′-(1-methylheptyloxycarbonyl)biphenyl-4-yl 4-(6-heptanoyloxyhex-1-oxy)benzoate where $R_1\equiv C_7H_{15}$ and $m=6$.

frequency limit of the permittivity and ε_0 is the permittivity of free space. The conductivity contribution expressed by the term $\frac{i\sigma_0}{2\pi\varepsilon_0 f^n}$ dominates in the low frequency range where σ_0 is the Ohmic conductivity and n a fitting parameter. The high frequency contribution to the spectra related to the resistance of the ITO layer is expressed by the term iAf^m where A and m are fitting parameters. The exponents n and m are close to one. However, the ITO skin conductivity problems can be avoided by using a measuring capacitor of suitable thickness and gold-plated electrodes. The dielectric data presented in the next section were obtained in this type of capacitor.

3. Results and discussion

Figure 2 shows a 3D plot of the temperature and frequency dependence of the relaxation losses in the AFLC. In the isotropic phase, besides the high frequency wing of the molecular process, the conductivity contribution related to ionic free charges present in the liquid crystal dominates. After the transition from the isotropic to the SmA phase one relaxation process is observed, which can be assigned to fluctuations of the tilt angle, known as a soft mode (SM). In the SmA–SmC* phase transition the soft mode splits into the soft amplitude mode and the Goldstone mode (GM) related to azimuthal angle fluctuations. The GM with very high dielectric strength covers the SM in the SmC* phase. With lowering temperature two additional modes appear in the antiferroelectric SmC_a^* phase, known as high frequency P_H and low frequency P_L modes [16, 30].

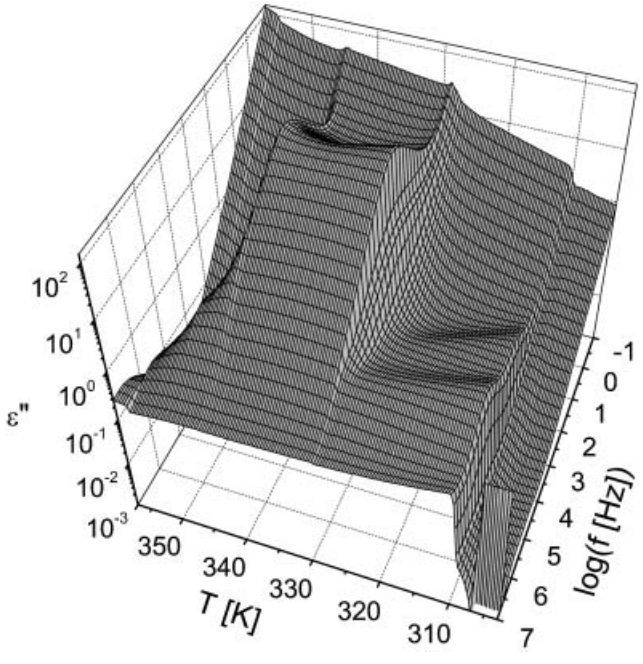

Figure 2. Three-dimensional plot of the temperature and frequency dependence of the dielectric losses in the antiferroelectric liquid crystal.

Figure 3 shows the temperature dependence of the real part $\varepsilon'(\omega, T)$ of the dielectric permittivity at different frequencies. The changes of $\varepsilon'(\omega, T)$ with temperature confirms the existence of several different mesophases in this AFLC. The characteristic increase of dielectric permittivity in the SmA–SmC* phase transition is related to the appearance of the soft mode in the SmA phase and the Goldstone mode in the SmC* phase. With increasing frequency, the value of the dielectric permittivity gradually decreases in the SmC* phase because the Goldstone mode is shifted away from the frequency window. However, the characteristic peak for the soft mode appears (see the logarithmic scale in the inset of figure 3) in the higher frequencies. The frequency changes of $\varepsilon'(\omega, T)$ in the $SmC^* - SmC_a^*$ phase transition indicates coexistence of the ferroelectric and antiferroelectric relaxation modes in this range of temperature (see inset in figure 3). In the antiferroelectric SmC_a^* phase the dielectric permittivity again attains a very low value, comparable to that in the isotropic phase.

Figure 4 shows the frequency dependence at $T=324$ K of the real $\varepsilon'(\omega, T)$ and imaginary $\varepsilon''(\omega, T)$ parts of the dielectric permittivity $\varepsilon^*(\omega, T)$ in the antiferroelectric SmC_a^* phase. The spectrum reveals the two well separated low frequency P_L and high frequency P_H relaxation processes. It is generally accepted that the P_L mode can be related to the in-phase and P_H to the anti-phase azimuthal angle fluctuations of the directors of the anti-tilted molecules in successive layers [16, 18, 30]. The data presented in figure 4 were fitted to equation (1) (only the three first terms) with $\Delta\varepsilon=0.56$, $\alpha=0.2$, $\gamma=1$ for the P_L relaxation process, and $\Delta\varepsilon=1.5$, $\alpha=0$, $\gamma=0.79$ for the P_H mode.

Figure 5 shows the temperature dependence of the characteristic relaxation frequency of the relaxation processes occurring in the investigated compound, and figure 6 shows the temperature dependence of the dielectric strength of these processes. The phase transition temperatures obtained from the dielectric spectra correspond almost perfectly to those taken from calorimetric measurements. In the SmA phase the characteristic temperature dependences of the relaxation frequency and dielectric strength for the soft mode are observed. The SM relaxation frequency decreases but its dielectric strength increases on approaching the SmA–SmC* transition temperature. In the SmC* phase the GM dominates with very high dielectric strength

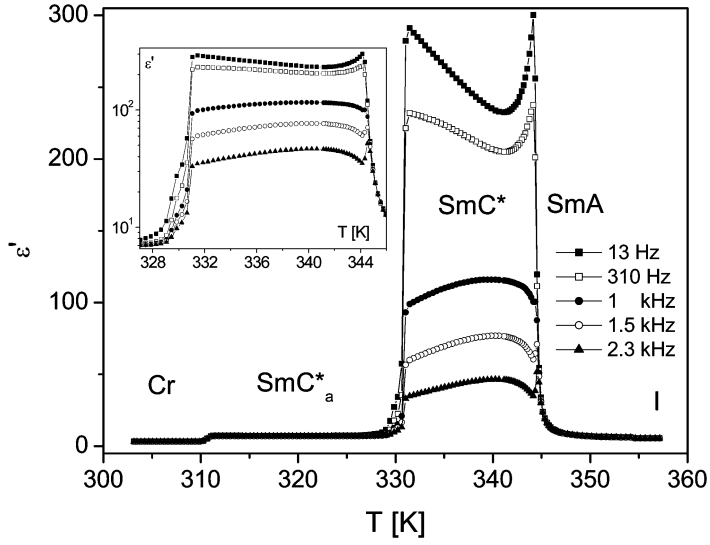

Figure 3. Temperature dependence of the dielectric dispersion at chosen frequencies.

(about 300) and with a relaxation frequency in the kHz range almost independent of the temperature.

The only possibility for extracting the soft mode from the spectrum in the SmC* phase is the application of a bias field to suppress the Goldstone mode. Therefore, the SmA–SmC* transition area was temperature-scanned with temperature steps of 0.2 deg in an electric field of strength of $0.7\,\mathrm{V\,\mu m^{-1}}$. The SM relaxation frequency and dielectric strength obtained in this way are shown in figures 5 and 6, together with data for the SmA phase. At a temperature of about 330.7 K a slight decrease of the GM relaxation frequency and a small decrease of dielectric strength are visible. In this area the GM relaxation process begins to disappear from the spectrum but at the same time the high frequency P_H process appears. In this range the relaxation frequency and dielectric strength of the P_H relaxation process are almost temperature independent. However, the characteristic bump at $T \sim 327\,\mathrm{K}$ on the temperature dependence of the GM frequency is visible. At about 324.7 K a new P_L mode appears in the spectrum but the GM disappears completely with decreasing temperature.

This coexistence of both processes is observed over a temperature range of several degrees and was also observed in an analogous antiferroelectric compound

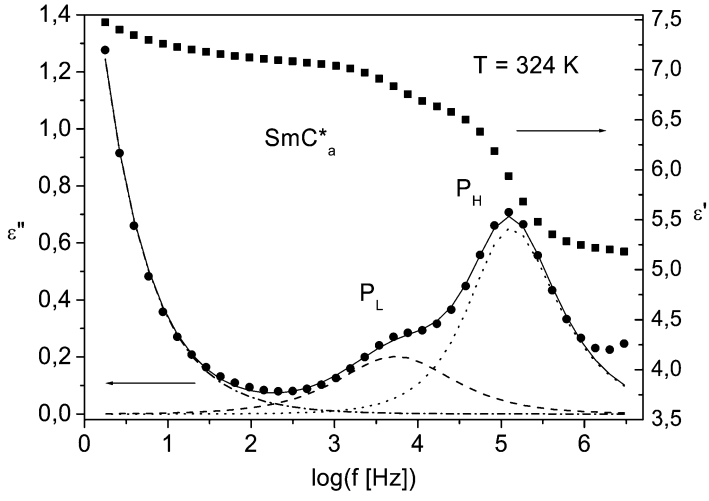

Figure 4. Frequency dependence of the real and imaginary parts of the dielectric permittivity in the antiferroelectric SmC_a^* phase at a chosen temperature. The solid line is a superposition of two Havriliak–Negami fits and conductivity contribution. Dashed lines represent deconvolution into elementary contributions.

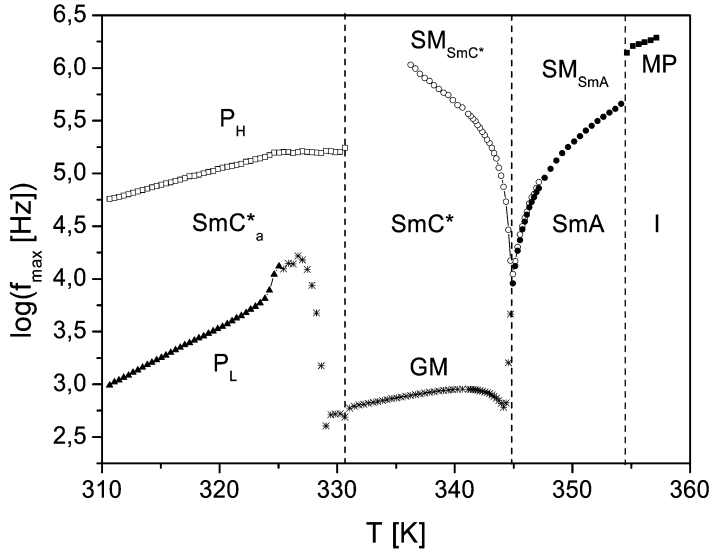

Figure 5. Temperature dependence of the characteristic relaxation frequencies of the relaxation processes observed in this antiferroelectric liquid crystal: MP=molecular process (solid squares), SM_{SmA}=the soft mode in the SmA phase (filled circles), SM_{SmC*}=soft mode in the SmC* phase in a bias electric field (open circles), GM=the Goldstone mode (stars), P_L=the low frequency AFLC mode (filled triangles), P_H=the high frequency AFLC mode (open squares).

with $R_1 \equiv C_6H_{13}$ and $m=6$ [30]. Below this temperature the P_L and P_H antiferroelectric modes appear simultaneously. The relaxation frequency f of both modes decreases almost linearly with temperature but the dielectric strength is only slightly temperature dependent. The dielectric strength $\Delta\varepsilon$ of the P_H mode is greater than that of the P_L mode and increases slightly, with decreasing temperature while for P_L it decreases. The described temperature dependence of $\Delta\varepsilon$ and f has been reported for several other antiferroelectric materials [16, 18, 30]. The temperature dependence of the relaxation frequency of both modes can be fitted to the Arrhenius law which gives an activation energy for the P_H mode of about 58 kJ mol^{-1} and for the P_L mode of about 111 kJ mol^{-1} (figure 7).

Figure 8 presents the temperature dependence of the soft mode dielectric strength and the characteristic relaxation frequency in the SmA and SmC* phases

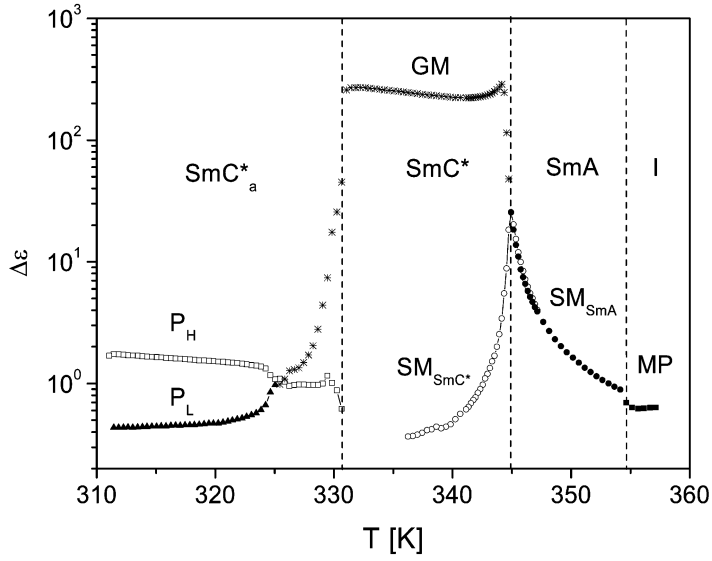

Figure 6. Temperature dependence of the dielectric strength of the relaxation modes present in this antiferroelectric liquid crystal. The symbols and acronyms are the same as in figure 5.

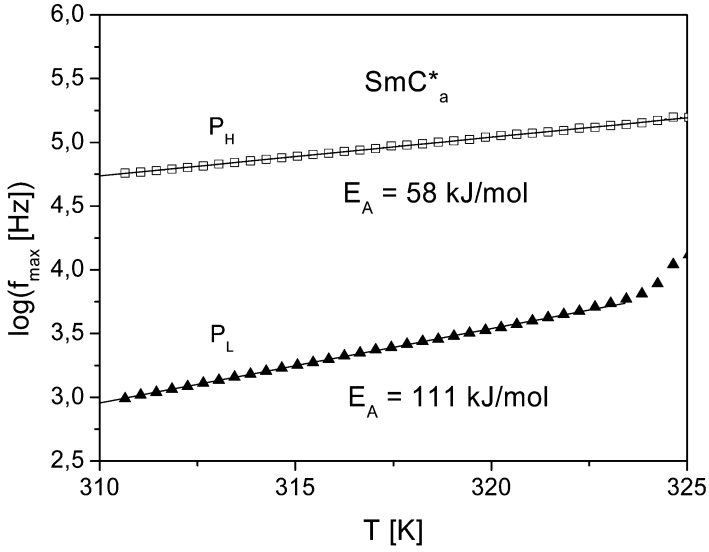

Figure 7. Temperature dependence of the characteristic frequency of the antiferroelectric modes. The lines are fittings with a straight line.

obtained with and without a bias field. In the SmC* phase a bias electric field of about $0.7\,\mathrm{V\,\mu m^{-1}}$ was applied to suppress the Goldstone mode which usually covers the much weaker soft mode. This enables analysis of the inverse of the soft mode dielectric strength on both sides of the SmA–SmC* phase transition. Figure 9 shows that the temperature dependence of $1/\Delta\varepsilon$ is linear in both phases. However, close to the SmA–SmC* transition some deviation from linearity is observed. In the SmA phase ($T \geqslant T_{\mathrm{AC}}$) the data can be fitted to the equation [31, 32]:

$$\varepsilon_0 \Delta\varepsilon_{\mathrm{s,\,A}} = \frac{\varepsilon^2 C^2}{a_0(T - T_{\mathrm{AC}}) + (K_3 - \varepsilon\mu^2)q_0^2} \tag{2}$$

where a_0 is a phenomenological constant of the Landau free energy density expansion, μ and C are coefficients of the flexoelectric and piezoelectric bilinear coupling, ε is the dielectric constant of the system in the high frequency limit, K_3 is the twist elastic constant and q_0 is the wave vector of the helix at $T = T_{\mathrm{AC}}$. From the fits to equation (2), which is represented as a straight line in figure 9, it can be deduced that for the phase transition temperature $T_{\mathrm{AC}} = 344.95\,\mathrm{K}$: $\dfrac{\varepsilon^2 C^2}{\varepsilon_0 a_0} = 8.3 \pm 0.2\,\mathrm{K}$ and $\dfrac{(K_3 - \varepsilon\mu^2)q_0^2}{a_0} = 0.22 \pm 0.02\,\mathrm{K}$. In the SmC* phase the soft mode dielectric strength can be fitted to the equation [33]:

$$\Delta\varepsilon_{\mathrm{s}} = \frac{1}{4a_0\varepsilon_0(T - T_{\mathrm{AC}}) + A}\left(\frac{b_3}{b_7}\right)^2 \tag{3}$$

where A is a cutoff term and b_3 and b_7 are parameters related to the biquadratic coupling between tilt and polarization. From fitting the experimental data to

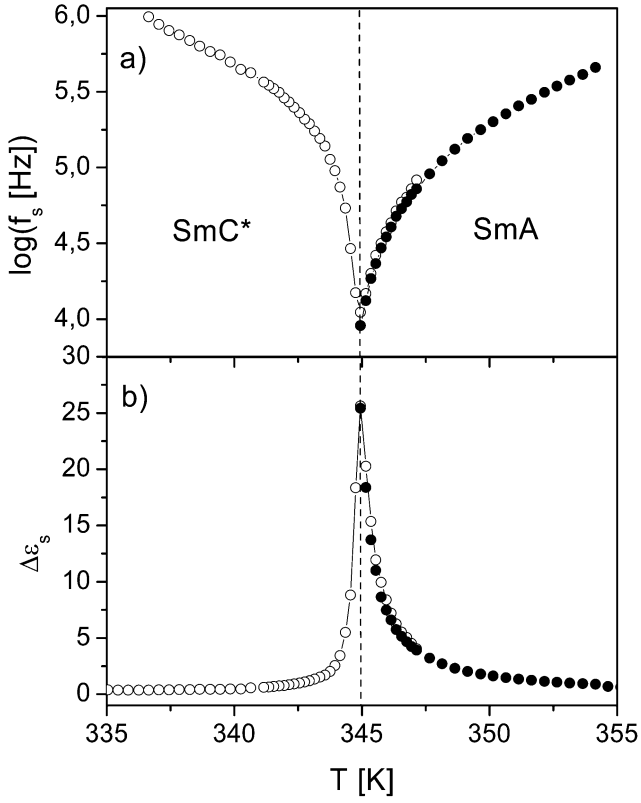

Figure 8. (*a*) Temperature dependence of the characteristic frequency, and (*b*) dielectric strength of the soft mode near the SmA–SmC* phase transition.

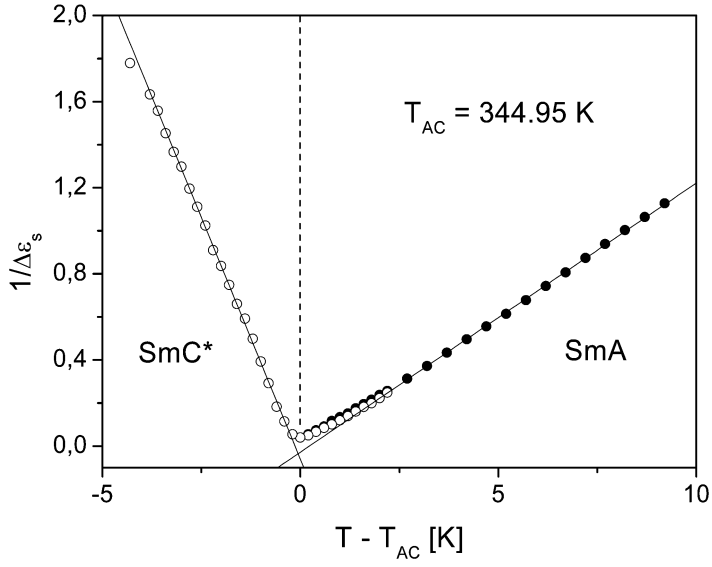

Figure 9. Temperature dependence of the inverse of the soft mode dielectric strength. The straight lines are fits to equation (3) in the SmA phase and to equation (3) in the SmC* phase.

equation (2) in the SmC* phase, the following values can be obtained: $\frac{4a_0\varepsilon_0}{(b_3/b_7)^2} = 0.45 \pm 0.01\ \mathrm{K}^{-1}$ and $\frac{A}{(b_3/b_7)^2} = 0.10 \pm 0.02$. Compared with the other available experimental data [33, 34] the order of magnitude of the obtained ratios of the different parameters seems to be reasonable. Other quantities involved in equations (2) and (3) can only be calculated after experimental determination of the temperature dependence of the tilt angle and spontaneous polarization. The appropriate measurements are in progress.

4. Conclusions

Broadband dielectric spectroscopy in the frequency range 10^{-2} to 10^7 Hz was applied to investigate dielectric relaxation processes in a newly synthesized antiferroelectric liquid crystal. In the paraelectric SmA phase the soft mode with characteristic changes in the relaxation frequency and relaxation dielectric strength was observed. In the ferroelectric SmC* phase the soft mode splits into the soft amplitude mode and the Goldstone mode. The soft mode relaxation frequency and dielectric strength in the SmC* phase were obtained by suppressing the Goldstone mode with an electric field. Some parameters involved in the extended Landau model of the SmA–SmC* phase transition were determined from analysis of the temperature dependence of the soft mode dielectric strength. The dielectric measurements reveal coexistence in the temperature range of several degrees of the Goldstone mode and P_H relaxation processes. This behaviour can result from the possible competition between synclinic and anticlinic order of the directors in the successive smectic layers. In the antiferroelectric SmC_a^* phase the low frequency process P_L is assigned to the in-phase fluctuations of the azimuthal angle, but the high frequency process P_H is assigned to anti-phase fluctuations of the azimuthal angle. The characteristic frequency of these processes follows the Arrhenius law.

It should be stated that in highly tilted AFLCs the cone angle approaches the magic value of 90°, which should probably be reflected in the dielectric behaviour of the antiferroelectric modes. This thesis can be confirmed or rejected in future experiments with a series of AFLC mixtures possessing different tilt angles changing in the range from 25° to 45°.

Acknowledgements

This work has been supported by the Fund for Scientific Research Flanders, Belgium (FWO, project G.0246.02). S.A.R. acknowledges the receipt of a senior post-doctoral fellowship from the Research Council of K.U.Leuven.

References

[1] S.T. Lagerwall. *Ferroelectric and Antiferroelectric Liquid Crystals*. Wiley-VCH, Weinheim (1999).
[2] J.P.F. Lagerwall, P. Rudquist, S.T. Lagerwall, F. Giesselmann. *Liq. Cryst.*, **30**, 399 (2003).
[3] J.P.F. Lagerwall, G. Heppke, F. Giesselmann. *Eur. Phys. J. E*, **18**, 113 (2005).

[4] W. Kuczyński, F. Goc, D. Dardas, R. Dąbrowski, J. Hoffmann, B. Stryła, J. Małecki. *Ferroelectrics*, **274**, 83 (2002).
[5] P. Rudquist, J.P.F. Lagerwall, J.G. Meier, K. D'havé, S.T. Lagerwall. *Phys. Rev. E*, **66**, 061708 (2002).
[6] G. Scalia, P. Rudquist, D.S. Hermann, K. D'havé, S.T. Lagerwall, J.R. Sambles. *J. appl. Phys.*, **91**, 9667 (2002).
[7] K. D'havé, P. Rudquist, S.T. Lagerwall, H. Pauwels, W. Drzewiński, R. Dąbrowski. *Appl.Phys. Lett.*, **76**, 3528 (2000).
[8] S. Lagerwall, A. Dahlgren, P. Jägemalm, P. Rudquist, K. D'havé, H. Pauwels, R. Dąbrowski, W. Drzewiński. *Adv. funct. Mater.*, **11**, 87 (2001).
[9] J. Gąsowska, R. Dąbrowski, W. Drzewiński, M. Flipowicz, J. Przedmojski, K. Kenig. *Ferroelectrics*, **309**, 83 (2004).
[10] R. Dąbrowski, J. Gąsowska, J. Otón, W. Piecek, J. Przedmojski, M. Tykarska. *Displays*, **25**, 9 (2004).
[11] J. Gąsowska, R. Dąbrowski, W. Drzewiński, K. Kenig, M. Tykarska, J. Przedmojski. *Mol.Cryst. liq.Cryst.*, **411**, 231 (2004).
[12] J. Gąsowska, J. Dziaduszek, W. Drzewiński, M. Flipowicz, R. Dąbrowski, J. Przedmojski, K. Kenig. *Proc. SPIE*, **5565**, 72 (2004).
[13] M. Tykarska, Z. Stolarz, J. Dziaduszek. *Ferroelectrics*, **311**, 51 (2004).
[14] K. D'havé, A. Dahlgren, P. Rudquist, J.P.F. Lagerwall, G. Andersen, M. Matuszczyk, S.T. Lagerwall, R. Dąbrowski, W. Drzewiński. *Ferroelectrics*, **244**, 115–128 (2000).
[15] M.B. Pandey, R. Dhar, V.K. Agrawal, R. Dąbrowski, M. Tykarska. *Liq. Cryst.*, **31**, 973 (2004).
[16] M. Buivydas, F. Gouda, G. Andersson, S.T. Lagerwall, B. Stebler, J. Bomelburg, G. Heppke, B. Gestblom. *Liq. Cyst.*, **23**, 723 (1997).
[17] V. Hamplova, A. Bubnov, M. Kaspar, V. Novotna, D. Pociecha, M. Glogarova. *Liq. Cryst.*, **30**, 627 (2003).
[18] Yu.P. Panarin, O. Kalinovskaya, J.K. Vij. *Liq. Cryst.*, **25**, 241 (1998).
[19] J.P.F. Lagerwall, D.D. Parghi, D. Krüerke, F. Gouda, P. Jägemalm. *Liq. Cryst.*, **29**, 163 (2002).
[20] S.K. Kundu, B.K. Chaudhuri, A. Seed, A. Jákli. *Phys. Rev. E*, **67**, 041704 (2003).
[21] J.W. O'Sullivan, J.K. Vij, H.T. Nguyen. *Liq. Cryst.*, **23**, 77 (1997).
[22] Yu.P. Panarin, O. Kalinovskaya, J.K. Vij, J.W. Goodby. *Phys. Rev. E*, **55**, 4345 (1997).
[23] R. Stannarius, Ch. Langer, W. Weissflog. *Phys. Rev. E*, **66**, 031709 (2002).
[24] V. Bourny, J. J. Pavel, V. Lorman, H.T. Nguyen. *Liq. Cryst.*, **27**, 559 (2000).
[25] M. Škarabot, R. Blinc, G. Heppke, I. Muševič. *Liq. Cryst.*, **28**, 607 (2001).
[26] P. Mach, R. Pindak, A.-M. Levelut, P. Barois, H.T. Nguyen, C.C. Huang, L. Furenlid. *Phys. Rev. Lett.*, **81**, 1015 (1998).
[27] P. Mach, R. Pindak, A.-M. Levelut, P. Barois, H.T. Nguyen, H. Baltes, M. Hird, K. Toyne, A. Seed, J.W. Goodby, C.C. Huang, L. Furenlid. *Phys.Rev. E.*, **60**, 6793 (1999).
[28] J. Philip, J.R. Lalanne, J.P. Marcerou, G. Sigaud. *Phys. Rev. E*, **52**, 1846 (1995).
[29] M. Škarabot, M. Čepič, B. Žekš, R. Blinc, G. Heppke, A.V. Kityk, I. Muševič. *Phys. Rev. E*, **58**, 575 (1998).
[30] G. Pandey, R. Dhar, V.K. Agrawal, R. Dąbrowski. *Phase Transitions*, **77**, 1111 (2004).
[31] C. Filipič, T. Carlsson, A. Levstik, B. Žekš, R. Blinc, F. Gouda, S.T. Lagerwall, K. Skarp. *Phys. Rev. A*, **38**, 5833 (1988).
[32] T. Carlsson, B. Žekš, C. Filipič, A. Levstik. *Phys. Rev. A*, **42**, 877 (1990).
[33] S. Merino, F. de Daran, M.R. de la Fuente, M.A. Perez Jubindo, T. Sierra. *Liq Cryst.*, **23**, 275 (1997).
[34] A. Kocot, R. Wrzalik, J.K. Vij, M. Brehmer, R. Zentel. *Phys. Rev. B*, **50**, 16346 (1994).